HIGH RESOLUTION TIME-OF-ARRIVAL FOR A CM-PRECISE SUPER 10 METER 802.15.3C-BASED 60 GHZ OFDM POSITIONING APPLICATION

Tom Redant[1] and Wim Dehaene[1,2]
[1]*ESAT-MICAS, K.U. Leuven, Kasteelpark Arenberg 10, B-3001 Leuven, Belgium*
[2]*IMEC, Kapeldreef 75, B-3001 Leuven, Belgium*

Keywords: Time-of-Flight Estimation, 60 GHz, 802.15.3c, NLOS-fading, High Resolution.

Abstract: A 802.15.3c-compatible technique for super 10 meter cm-accurate and precise ranging is introduced, achieving update rates of more than 300 kHz. The implementation is realized on top of the 802.15.3c PHY High-Speed-Interface mode, specifying a multi-carrier orthogonal frequency division multiplexed (OFDM) implementation. The aimed application conditions foresee strong discrete non-line-of-sight fading conditions. The system's performance is evaluated over these strong channel conditions. Due to the high absorption in the 60 GHz band and thus the poor signal-to-noise ratio at super 10 m distances the algorithm should be noise tolerant. The algorithm combines a classic auto correlation with the MLS-Prony method, a high resolution technique for frequency content analysis.

1 INTRODUCTION

Wireless Personal Area Networks (WPANs) are emerging in today's electronic devices, achieving super Gbit/s data rates over sub-10 m distances. The recent 802.15.3c PHY standard (IEEE, 2009) specifies a high speed interface mode (HSI), achieving these super Gbit/s data rates, using orthogonal frequency division multiplexing (OFDM) instead of a single carrier (SC) operation mode. The 802.15.3c HSI standard specifies a bandwidth B of 2.64 GHz for signals $u(t)$ at a carrier frequency f_c of 60 GHz and is therefore extremely suited for Time-of-Flight (ToF) and Time-of-Arrival (ToA) estimation, as Eqn. (1) of (Quazi, 1981) states.

$$\sigma_{\text{ToA}} \leq K_\beta \left(\frac{1}{T}\right)^{1/2} \frac{1}{SNR^\beta} \cdot \frac{1}{\sqrt{(f_c+B/2)^3-(f_c-B/2)^3}} \quad (1)$$

This equation represents the Cramér-Rao lower (CR) bound for the precision of passive ToF based radar applications in the presence of white Gaussian noise. $\beta = 1/2$ for high SNR values and $\beta = 1$ for low SNR values. It shows the inverse relationship of the ranging precision standard deviation σ_{ToA} and the signal's bandwidth B, carrier frequency f_c the signal's signal-to-noise ratio (SNR) and its duration T. K_β is a β depending proportionality constant. However, this equation assumes that the complete bandwidth contains a flat power allocation. The 802.15.3c HSI PHY standard is OFDM-based and the CR bound of this discrete carrier implementation is expected to enable ranging applications at a slightly reduced precision with respect to the flat power allocation. This paper will analyze the CR bound for OFDM-based ranging systems in the 60 GHz band based on the 802.15.3c HSI PHY standard.

Although, maximum propagation distances are around 10 m for the 802.15.3c HSI PHY standard, using an appropriate ToA estimation algorithm can push the suitability of the 802.15.3c HSI PHY specification towards higher distances, as is wanted for the application of interest. Moreover, the authors' application specifies strong discrete multipath propagation, asking for a multipath tolerant algorithm. High update rates are required and thus $1/T$ will be high. The effect of the small time window T is compensated by the broad bandwidth of the 802.15.3c HSI PHY. For the sake of reducing implementation costs, no multiple antenna techniques are considered for the application of interest.

The relation between the baseband received signal y(t), the ideally transmitted baseband signal $u(t)$, the channel noise $n(t)$ and the baseband-equivalent channel impulse response $h(t)$ is as shown in Eqn. (2).

Redant T. and Dehaene W..
HIGH RESOLUTION TIME-OF-ARRIVAL FOR A CM-PRECISE SUPER 10 METER 802.15.3C-BASED 60GHZ OFDM POSITIONING APPLICATION.
DOI: 10.5220/0003730302710277
In *Proceedings of the 2nd International Conference on Pervasive Embedded Computing and Communication Systems* (PECCS-2012), pages 271-277
ISBN: 978-989-8565-00-6

$$y(t) = h(t) * u(t) + n(t) = \int_0^\infty h(\tau) \cdot u(t-\tau) d\tau + n(t) \quad (2)$$

For typical indoor non-line-of-sight (NLOS) conditions, where the line-of-sight (LOS) component faces obstacles, the baseband equivalent channel impulse responses can be identified as:

$$h(t) = \sum_{i=0}^{M-1} A_i \cdot \delta(t - t_i) \cdot e^{-j \cdot 2\pi f_c t} \quad (3)$$

with $\exists A_i : A_i \approx A_0$ for NLOS conditions. A_i are the tap gains, t_i the tap time instants, M the number of multipath components j is the imaginary unit. As a good approximation, and for simulation purposes, this can be modeled as: $h(t) = \sum_{i=0}^{M} A_i \cdot \delta(t - t_i) \cdot e^{j \cdot \theta_i}$, with θ_i uniformly distributed in $[0, 2\pi)$. The baseband equivalent $h(t)$ is a complex function.

High resolution techniques enable higher ranging precisions than is enabled by the sample rate of the receiver system. (Neri et al., 2010) introduces a high resolution technique based on Kalman filters estimating the ToA. However, no NLOS-channel-aware techniques are implemented to cancel channel effects. (Xu et al., 2008) introduces a high resolution least squares based technique providing good results for frequency hopping OFDM applications. Due to 802.15.3c HSI PHY standard limitations, no frequency hopping is considered here. This paper will focus on the high resolution technique listed in (Tufts and Kumaresan, 1982). This algebraic technique can be applied to get a high resolution view on the channel behavior, the impulse response $h(t)$. This is done by examining the discretized impulse response estimate $\hat{h}[k]$ of $h[k] = h(k \cdot T_s)$ (T_s the sample rate)(Winter and Wengerter, 2000).

Section 2 shows insights on OFDM-based ranging, moreover introduces a CR-bound for this multi-carrier way of ranging. Section 3 describes the 802.15.3c compatible ranging package structure for the application. Section 4 and 5 respectively introduce the coarse and fine ToA estimation steps in order to come to a precise and accurate ToA figure. Section 6 evaluates the algorithm's results for a real channel and crystal offset values. Conclusions are drawn in section 7.

2 OFDM-BASED RANGING

Ranging applications clasically use single-carrier (SC) methods in order to find the ToA. The fact that OFDM is a good data carrier partially motivates its choice for a ranging application since hardware for both data communications and ranging can then be combined. However, OFDM's inherent ranging abilities need to be verified first. An evaluation of the CR-bound for the 802.15.3c HSI PHY spec needs to be carried out. In order to find this CR-bound, the general expression Eqn. (4) of (Knapp and Carter, 1976) needs to be evaluated:

$$\sigma_{\text{ToA}} \geq \left(2 \cdot T \cdot \int_0^\infty (2 \cdot \pi \cdot f)^2 \frac{|\gamma(f)|^2}{1 - |\gamma(f)|^2} df \right)^{-1} \quad (4)$$

with:

$$|\gamma(f)|^2 = \frac{G_{uu}^2(f)}{(G_{uu}(f) + G_{nn}(f))^2}.$$

$G_{uu}(f)$ and $G_{nn}(f)$ are respectively the PSD of the ranging signal and the uncorrelated noise. This expression will be evaluated for white noise and the discrete OFDM carrier allocation. According to (Liu and Li, 2004), the PSD of an OFDM package is:

$$G_{uu}(f) = K \cdot \sum_{-N/2}^{N/2-1} |W(f - f_c - k \cdot \Delta f)|^2 \quad (5)$$

K is a proportionality constant. $W(f)$ is the Fourier transform of the window function for the OFDM symbol. In an OFDM receiver, over the period of this window, a discrete fourier transform (DFT) is carried out. For a block pulsed window function of duration T_{DFT} this results into:

$$|W(f)|^2 = \frac{\sin^2(\pi f T_{\text{DFT}})}{\pi^2 f^2 T_{\text{DFT}}^2}. \quad (6)$$

The integral in Eqn. (4) cannot be evaluated analytically. Instead, a numerical evaluation of this bound will provide insights for the ranging abilities of the 802.15.3c HSI PHY. The time domain over which the ranging precision is evaluated is $T_{\text{DFT}} = 202\,\text{ns}$, the duration of one 802.15.3c OFDM package. All 336 available data sub carriers (see Table 1 for details) are assumed to have equal energy, including the static modulations on the 16 pilot tones. A time domain raised cosine windowing with rise time $T_r = 0.01 \cdot T$ is chosen. The bound is plot in Fig. 1 as a function of the signal's SNR. It is compared to the flat frequency band CR-bound (Quazi, 1981) having equal signal power. The CR-bound for the 802.15.3c HSI PHY spec is roughly equal to the flat frequency band case and doesn't suffer performance degradation compared to the flat spectrum case. Using OFDM for ranging is thus motivated.

3 PACKAGE STRUCTURE

So far, a theoretical analysis on the ranging abilities of the 802.15.3c OFDM signals was carried out in this

Table 1: Frequency domain sub carrier allocation for the 802.15.3c HSI PHY OFDM spec.

Sub carriers type	**Number of sub carriers**	**Logical sub carriers indexes**
Zero sub carriers	160	$[-256:-178]\cup[-1,0,1]\cup[178:255]$
Pilot sub carriers	16	$[-166:22:-12]\cup[12:22:166]$
Data sub carriers	336	All others

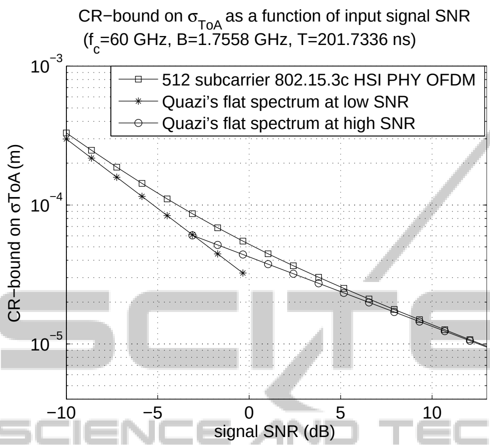

Figure 1: CR-bound for the 802.15.3c HSI PHY specification compared to the flat bandwidth allocation approximation of (Quazi, 1981)

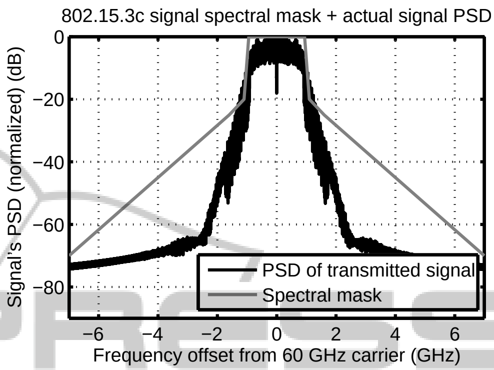

Figure 2: Power spectral density of the transmitted signal. The transmit filter is modeled by the 5th order Butterworth filter having a cutoff frequency of $\frac{178}{512}\cdot B/2$.

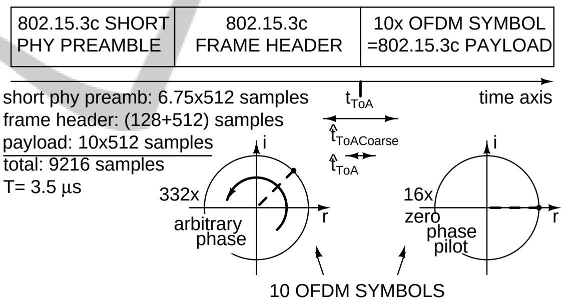

Figure 3: The considered ranging package. 10 OFDM symbols are appended to the 802.15.3c HSI PHY preamble. All 32 data sub carriers are equal gain and arbitrary phase modulated. The 16 pilot sub carriers are modulated by all ones.

paper. This section introduces the package structure which will be used in the process of ToA estimation. Moreover, so far, only white Gaussian noise perturbations were considered as a performance limiting effect on the σ_{ToA}. Since the ranging method should be tolerant to discrete multipath conditions, channel estimation should be carried out and the package should have dedicated fields for this. The 802.15.3c preamble enables channel estimation techniques based on Golay sequences. However, due to noise corruption of the received signals at super-10 m distances, this built-in short sequence does not provide enough averaging to suppress the noise in the aimed application. This is why the authors introduced $N_{\text{DFT}} = 10$ identical payload OFDM symbols of 512 samples, trailing the preamble. All N_{DFT} OFDM symbols' sub carriers are modulated by $1\cdot e^{j\cdot\alpha_i}$, with each α_i an arbitrary phase, known by the receiver's back-end. The α_i values can be chosen in a way the peak-to-average power ratio (PAPR) is low to tackle non-linearity issues in both transmit and receive paths. Additionally, the extra 16 pilot tones are modulated by ones. No guard interval is applied between consecutive OFDM symbols. Channel estimation and compensation can now be carried out using these N_{DFT} additional OFDM symbols. The 5th order Butterworth filter with cutoff frequency $\frac{178}{512}\cdot B/2$ is used to satisfy the spectral mask criterion (Fig. 2). Satisfying the specifications' spectral mask is an important action, yet, it is often omitted in algorithmic papers. The complete package structure is visualized in Fig. 3. The figure also defines the position of the t_{ToA}, being the time stamp on which the first payload OFDM symbol is received.

4 AUTO CORRELATION AS COARSE TOA ESTIMATION

The here-applied ToA estimation is based on aligning the (discrete Fourier transform) DFT window to the N_{DFT} OFDM symbols, trailing the preamble. However, due to the high amount of identical trailing OFDM symbols, this alignment procedure can result in a misalignment by $k \cdot T_{\mathrm{DFT}}$, with k an integer and T_{DFT} the OFDM symbol duration. This is why an initial coarse timing estimate $\hat{t}_{\mathrm{ToA\,Coarse}}$, positioning this DFT window, should lie in the interval $[t_{\mathrm{ToA}} - \frac{T_{\mathrm{DFT}}}{2} \ldots t_{\mathrm{ToA}} + \frac{T_{\mathrm{DFT}}}{2}]$. For this coarse timing estimate an auto correlation operation is preferred. The definition of the auto correlation for the signal $y[k]$ is shown in Eqn. (7) and Fig. 4. $\Delta k = 128$ is the window over which auto correlation is carried out and the *-operator represents the complex conjugation.

$$\begin{aligned}
\mathrm{def:} \quad r_{\mathrm{u}}[k] &= \sum_{i=k}^{k+\Delta k} u[i] \cdot u[i+\Delta k]^* \\
r_{\mathrm{y}}[k] &= \underbrace{|h[0]|^2 \cdot \sum_{i=k}^{k+\Delta k} u[i] \cdot u[i+\Delta k]^*}_{\text{Wanted contribution}} + n'[k] \qquad (7) \\
&+ \sum_{l=1}^{M} \sum_{m=1}^{M} h[l] \cdot h[m]^* \sum_{i=k}^{k+\Delta k} u[i-l] \cdot u[i-m]^*
\end{aligned}$$

The $\hat{t}_{\mathrm{ToA\,Coarse}}$ is found by detecting a phase jump of π in the auto correlation phase. Fig 5 shows the 802.15.3c HSI PHY preamble and the amplitude and phase output of the auto correlation. The dashed line in the correlation phase realizes a fixed time difference with the ToA coarse estimate as is indicated in (Fig. 3). The reason why an auto correlation is preferred is that this operation is generally known to be less susceptible to fading channel conditions than cross correlation based synchronizations (K. Wang and Tolochko, 2003). However, one should be aware of the fact that the auto correlation expression shows a $|h(0)|^2$-gain for the LOS component, stressing the NLOS components' gain with respect to the weaker $h[0]$-LOS component when facing a severe NLOS propagation. Whereas using the cross correlation (the LOS component has a gain of $h[0]$), this NLOS-stressing does not occur under severe NLOS conditions since it is a linear operation.

5 HIGH RESOLUTION TECHNIQUE AS FINE TOA ESTIMATION

The initial auto correlation based coarse ToA estimate is important for the high resolution technique. For this technique a frequency domain content analysis is performed and thus a DFT window needs to be positioned in an accurate way.

For pure data recovery, synchronization of the DFT window is not a critical issue to obtain channel information, thanks to the cyclic prefix. A malpositioning of the DFT window by ΔT_{DFT} causes the signal's frequency domain taps' phase to be shifted linearly by a slope $2 \cdot \pi \cdot \frac{\Delta T_{\mathrm{DFT}}}{T_{\mathrm{DFT}}}$, T_{DFT} representing the time window over which the DFT is performed. For ToA estimation, knowing this linear phase perturbation is a main concern. In order to identify the linear phase contribution caused by a misaligned DFT, a simple linear regression on the frequency domain taps phases seems to be sufficient. However, when facing severe channel multipath components, an elaborated analysis of the estimated impulse response $\hat{h}[k]$ or its frequency domain version $\hat{\mathbf{H}}$ is needed. High resolution techniques based on identifying the frequency content (Tufts and Kumaresan, 1982) of the frequency domain channel taps $\hat{\mathbf{H}}$ bring a solution. In (Winter and Wengerter, 2000) the Modified-Least-Squares-Prony method (MLS-Prony), based on linear prediction modeling and noise reduction, is applied to GSM signals improving ranging capabilities of a mobile phone based ToA ranging system. In this paper, it is used as a fine-tuning step after finding the coarse auto correlation based timing estimate. It is applied to 802.15.3c HSI signals, dealing with the finite knowledge of the frequency domain impulse response due to the inherent notches by the presence of guard carriers. The MLS-Prony method is applied to the frequency domain channel taps, the $\hat{\mathbf{H}}$ vector:

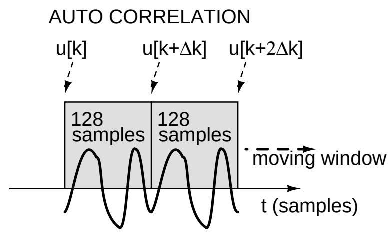

Figure 4: Illustration of the auto correlation operation.

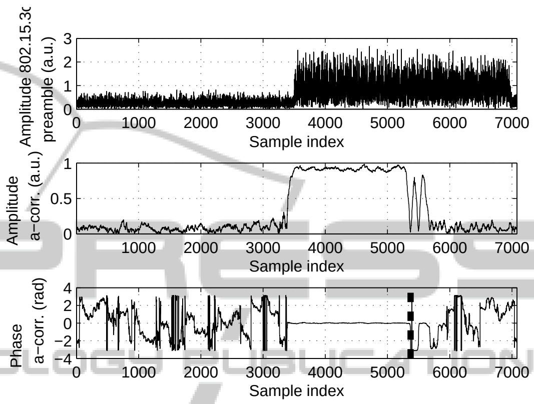

Figure 5: The auto correlation applied to the 802.15.3c HSI PHY preamble.

$$N_{\text{DFT}} \cdot \hat{\mathbf{H}} = \sum_{i=1}^{N_{\text{DFT}}} \frac{\mathcal{F}\left[y[\hat{k}_s + 512(i-1)], \ldots, y[\hat{k}_s + 512i - 1]\right]}{\mathcal{F}\left[u[\hat{k}_s + 512(i-1)], \ldots, u[\hat{k}_s + 512i - 1]\right]}$$
$$\text{with}: \qquad \hat{k}_s = \frac{\hat{t}_{\text{ToACoarse}}}{T_s}. \tag{8}$$

The $\mathcal{F}$ operation represents the 512-point DFT. The $\hat{\mathbf{H}}$ vector is realized by a tap-by-tap division of two 512 tap DFT vectors. In order to match the sub carrier allocation of Table 1, the $\hat{\mathbf{H}}$ vector is indexed -256..255. Due to the inherent notches in the sub carrier spectrum, a limited scope on this frequency domain taps is provided.

The high resolution method itself (Winter and Wengerter, 2000) is based on identifying the linear prediction filter with length L producing the $\hat{\mathbf{H}}$ samples. The zeros r_i of the prediction error filter are complex and those close to the unit circle represent the $\hat{\mathbf{H}}$ vector's frequency content, which is related to the time domain impulse response $\hat{h}[k]$'s multipath time instances and thus the ToA. The root with the lowest phase value defines the line of sight component and thus provides a correction to the initial $\hat{t}_{\text{ToA Coarse}}$ timing estimate:

$$\hat{t}_{\text{ToA}} = \min_{\text{i}} \left(\frac{N \cdot T_s}{2 \cdot \pi} \angle(r_i) \right) + \hat{t}_{\text{ToA Coarse}} \tag{9}$$

The $\angle$-operator represents the complex angle. In this work, a maximum correction ability $|\hat{t}_{\text{ToA Coarse}} - \hat{t}_{\text{ToA}}|$ for the MLS-Prony method is applied, according to the performance of the $\hat{t}_{\text{ToA Coarse}}$ estimation. The interval $[\frac{-10\,\text{m}}{c}, \frac{10\,\text{m}}{c}]$ seems reasonable for the auto correlation implementation. c is the speed of light. $T_s = 1/[2.64\,\text{GHz}]$ represents the receiver sample rate, N the number of samples of the signal to which the MLS-Prony method is applied.

The here-proposed modification of the MLS-Prony algorithm is based on the matrix A. This data matrix A, which is needed in the process to identify the linear prediction filter, should only be filled by the corresponding non-zero $\hat{\mathbf{H}}$ values. Therefore, it is constructed based on the concatenation of 2 data matrices based on respectively the lower and higher non-zero 176 frequency domain taps. Eqn. (11) defines this matrix.

$$A^T = \left[A^T_{\text{low}} \; A^T_{\text{high}}\right] =$$
$$\begin{bmatrix} \hat{\mathbf{H}}_{-168} & \cdots & \hat{\mathbf{H}}_{-3} & \hat{\mathbf{H}}^*_{-176} & \cdots & \hat{\mathbf{H}}^*_{-11} & \hat{\mathbf{H}}_{11} & \cdots & \hat{\mathbf{H}}_{176} & \hat{\mathbf{H}}^*_{3} & \cdots & \hat{\mathbf{H}}^*_{168} \\ \vdots & \ddots & \vdots & \vdots & \ddots & \vdots & \vdots & \ddots & \vdots & \vdots & \ddots & \vdots \\ \hat{\mathbf{H}}_{-177} & \cdots & \hat{\mathbf{H}}_{-12} & \hat{\mathbf{H}}^*_{-167} & \cdots & \hat{\mathbf{H}}^*_{-2} & \hat{\mathbf{H}}_{2} & \cdots & \hat{\mathbf{H}}_{167} & \hat{\mathbf{H}}^*_{12} & \cdots & \hat{\mathbf{H}}^*_{177} \end{bmatrix} \tag{10}$$

The ^{T} operator represents the matrix transpose. The H matrix for the algorithm of (Winter and Wengerter, 2000) will be reformed into:

$$H^T = \left[H^T_{\text{low}} \; H^T_{\text{high}}\right] =$$
$$\left[\hat{\mathbf{H}}_{-167} \cdots \hat{\mathbf{H}}_{-2} \; \hat{\mathbf{H}}_{-177} \cdots \hat{\mathbf{H}}_{-12} \; \hat{\mathbf{H}}_{12} \cdots \hat{\mathbf{H}}_{177} \; \hat{\mathbf{H}}_{2} \cdots \hat{\mathbf{H}}_{167}\right]$$

In order to reduce the computational complexity, no noise reducing singular value decomposition is carried out on the A matrix.

6 SIMULATION RESULTS

An algorithmic Matlab model of the transmitter, channel and receiver is implemented according to the design decisions as presented in sections 3, 4 and 5. The channel is modeled by a random additive white Gaussian noise contribution (AWGN) and multipath propagation according to Eqn. (3). The considered impulse response is shown in Eqn. (11).

$$h(t) = 0.25 \cdot \delta(t) \cdot e^{j \cdot \theta_1} + \delta(t - \frac{5\,\text{m}}{c}) \cdot e^{j \cdot \theta_2} + \delta(t - \frac{6\,\text{m}}{c}) \cdot e^{j \cdot \theta_3} + \delta(t - \frac{7.5\,\text{m}}{c}) \cdot e^{j \cdot \theta_4} \tag{11}$$

Transmitter-receiver crystal frequency mismatch, resulting in carrier frequency offset (CFO) and sampling clock offset (SCO) is modeled. No Doppler frequency shift is considered since the application's wireless nodes move at low speed. This means that CFO and SCO perturbations are equal, and linked by the shared receiver's crystal. This work assumes a CFO estimation and compensation as is proposed in (Moose, 1994). This is a straightforward approach. Iterative, and joint timing and frequency synchronization approaches are available (Minn et al., 2003), (Abdzadeh-Ziabari and G. Shayesteh, 2011) but they come at an increased computation cost. Moreover, (Minn et al., 2003) makes abstraction of the SCO. After frequency offset compensation, the resulting frequency error is a function of the received signal's Signal-to-Noise-Ratio (SNR_y) and satisfies the conditions for its mean (μ) and its standard deviation (σ) as is shown in Eqn. (12).

$$\begin{aligned} \mu[\hat{\varepsilon} - \varepsilon \mid \varepsilon] &= 0 \\ \sigma^2[\hat{\varepsilon} - \varepsilon \mid \varepsilon] &= \frac{1}{4\pi^2 \cdot \text{SNR}_y \cdot \Delta T_{\text{estim}}/2 \cdot B} \end{aligned} \tag{12}$$

ε en $\hat{\varepsilon}$ are the normalized actual and estimated frequency offset. ΔT_{estim} is the time window over which the frequency offset is estimated. The SYNC field of the PHY preamble consists of 14 code repetitions of the 128 sample $\mathbf{a}_{128}$, and therefore $\Delta T_{\text{estim}} = 14 \cdot 128 \cdot T_s = 679\,\text{ns}$. These formulae provide interesting information on the expected amount of frequency mismatch. (Moose, 1994), (Pollet et al., 1995) and (Pollet et al., 1994) all provide formulae, expressing the effect of a resulting CFO and SCO as an SNR-degradation to the signal, modeling the inter carrier interference (ICI) and inter symbol interference (ISI). However, in this work the resulting CFO and SCO are applied to the signal $y[k]$ according its definition in Eqn. (13), providing signal $y'[k]$, which is fed to the algorithm. This approach enables realistic simulation results.

$$y'[k] = y(t) \cdot e^{j\cdot 2\cdot \pi(\hat{\varepsilon}-\varepsilon)\cdot[60GHz]\cdot t}\big|_{t=k\cdot T_s\cdot(1+(\hat{\varepsilon}-\varepsilon))} \quad (13)$$

Fig. 6 shows the technique's ToA performance figures. For each input SNR value (20 dB down to 3 dB), 1000 different sets $\{\theta_1, ..\theta_4\}$ for the NLOS-AWGN-channel of Eqn. (11) are evaluated and both a good precision and accuracy is achieved. For the sake of comparison, the auto correlation based $\hat{t}_{\text{ToA Coarse}}$ is also evaluated. The auto correlation operation is normalized in order to compensate for channel gain variations (K. Wang and Tolochko, 2003). Its performance is more-or-less constant over the AWGN-SNR range, but it faces an overestimation of more than 6 m due to the time-spread caused by the discrete multipath components. The here-proposed method shows a cm-accurate and precise ToA estimation at the lowest SNR values. These values correspond to distances over 10 m.

7 CONCLUSIONS

In this paper, the ranging abilities for the 802.15.3c HSI PHY OFDM standard are evaluated in order to enable an integrated 60 GHz cm-ranging/data communications system. A general evaluation of the OFDM ranging capabilities is performed. A ranging method for non-frequency locked, frequency offset compensating, wireless nodes is introduced. The MLS-Prony high resolution technique is an interesting tool and implies cm-precise and accurate ranging for discrete multipath NLOS-conditions at 60 GHz 802.15.3c HSI WPAN, using a single antenna. The MLS-Prony data matrix is modified in order to deal with zero sub carriers. The technique still performs well at SNR values close to 3 dB. 10 additional OFDM-packages are added to the HSI preamble, achieving a total package length of 3.5 μs, realizing a super 300 kHz update rate.

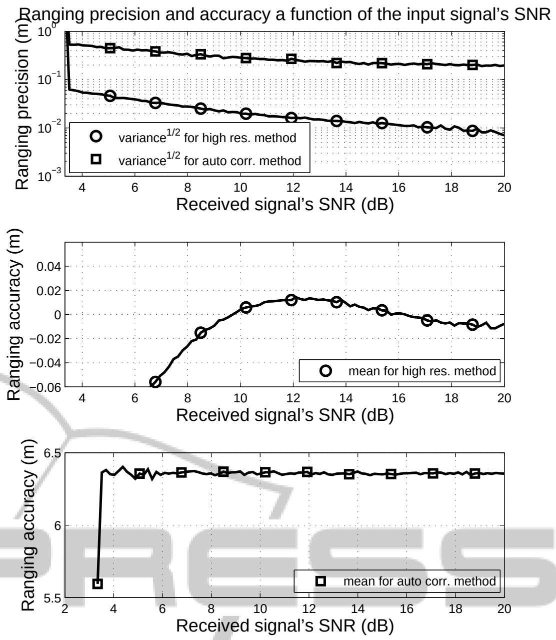

Figure 6: Accuracy ($|\hat{t}_{\text{ToA}} - t_{\text{ToA}}|$) and precision $\sqrt{\text{Var}(\hat{t}_{\text{ToA}} - t_{\text{ToA}})}$ as a function of the received signal's SNR for the high resolution MLS-Prony method and the auto correlation. Both methods face a positively biased ranging error due to the trailing multipath energy.

ACKNOWLEDGEMENTS

The authors would like to thank the Flemish agency for Innovation by Science and Technology (IWT) and the company ESSENSIUM NV for the funding. Moreover, they thank E. Van Lil, P. A. J. Nuyts and N. De Clercq for the interesting discussions.

REFERENCES

Abdzadeh-Ziabari, H. and G. Shayesteh, M. (2011). Robust timing and frequency synchronization for OFDM systems. *Vehicular Technology, IEEE Transactions on*, PP(99):1.

IEEE (2009). IEEE standard for information technology - telecommunications and information exchange between systems - local and metropolitan area networks - specific requirements. part 15.3: Wireless medium access control (MAC) and physical layer (PHY) specifications for high rate wireless personal area networks (WPANs) amendment 2: Millimeter-wave-based alternative physical layer extension. *IEEE Std 802.15.3c-2009 (Amendment to IEEE Std 802.15.3-2003)*, pages c1 –187.

K. Wang, M. Faulkner, J. S. and Tolochko, I. (2003). Timing synchronization for 802.11a WLANs under multipath channels. In *Australasian Telecommunication*

Networks And Applications Conference 2003, ATNAC 2003.

Knapp, C. and Carter, G. (1976). The generalized correlation method for estimation of time delay. *Acoustics, Speech and Signal Processing, IEEE Transactions on*, 24(4):320 – 327.

Liu, C. and Li, F. (2004). Spectrum modelling of OFDM signals for WLAN. *Electronics Letters*, 40(22):1431 – 1432.

Minn, H., Bhargava, V., and Letaief, K. (2003). A robust timing and frequency synchronization for OFDM systems. *Wireless Communications, IEEE Transactions on*, 2(4):822 – 839.

Moose, P. (1994). A technique for orthogonal frequency division multiplexing frequency offset correction. *Communications, IEEE Transactions on*, 42(10):2908 – 2914.

Neri, A., Di Nepi, A., and Vegni, A. (2010). DOA and TOA based localization services protocol in IEEE 802.11 networks. *Wireless Personal Communications*, 54:155–168. 10.1007/s11277-009-9719-y.

Pollet, T., Spruyt, P., and Moeneclaey, M. (1994). The BER performance of ofdm systems using non-synchronized sampling. In *Global Telecommunications Conference, 1994. GLOBECOM '94. Communications: The Global Bridge., IEEE*, pages 253 –257 vol.1.

Pollet, T., Van Bladel, M., and Moeneclaey, M. (1995). BER sensitivity of OFDM systems to carrier frequency offset and wiener phase noise. *Communications, IEEE Transactions on*, 43(234):191 –193.

Quazi, A. (1981). An overview on the time delay estimate in active and passive systems for target localization. *Acoustics, Speech and Signal Processing, IEEE Transactions on*, 29(3):527 – 533.

Tufts, D. and Kumaresan, R. (1982). Estimation of frequencies of multiple sinusoids: Making linear prediction perform like maximum likelihood. *Proceedings of the IEEE*, 70(9):975 – 989.

Winter, J. and Wengerter, C. (2000). High resolution estimation of the time of arrival for gsm location. In *Vehicular Technology Conference Proceedings, 2000. VTC 2000-Spring Tokyo. 2000 IEEE 51st*, volume 2, pages 1343 –1347 vol.2.

Xu, H., Chong, C.-C., Guvenc, I., Watanabe, F., and Yang, L. (2008). High-resolution TOA estimation with multi-band OFDM UWB signals. In *Communications, 2008. ICC '08. IEEE International Conference on*, pages 4191 –4196.